Original Article

The Effect of ZnO Nanoparticles Functionalized with Glutamine and Conjugated with Thiosemicarbazide on Triggering of Apoptosis in the Adenocarcinoma Gastric Cell Line

Sadaf Beigi[1], Ali Salehzadeh[1], Hadi Habibollahi[1], Seyed Ataollah Sadat Shandiz[2], Fariba Safa[3]

[1]Department of Biology, Rasht Branch, Islamic Azad University, Rasht, Iran, [2]Department of Biology, Central Tehran Branch, Islamic Azad University, Tehran, Iran, [3]Department of Chemistry, Rasht Branch, Islamic Azad University, Rasht, Iran

Abstract

Background: Gastric carcinoma is the fourth most common malignancy worldwide. Conjugation of metal nanoparticles with thiosemicarbazones has shown considerable anti-cancer potential.

Materials and Methods: Zinc oxide nanoparticles (ZnO NPs) were synthesized, functionalized by glutamine, and conjugated with thiosemicarbazide (ZnO@Gln-TSC). Fourier transform infrared spectroscopy, X-ray diffraction, scanning electron microscopy and transmission electron microscopy imaging, energy-dispersive X-ray, DLS, and zeta potential were used to characterize the NPs. The toxicity of ZnO NPs, TSC, ZnO@Gln-TSC NPs, and oxaliplatin in AGS cells and ZnO NPs and ZnO@Gln-TSC NPs in HEK293 cells was investigated by MTT assay. Cell apoptosis was evaluated by flow cytometry, caspase-3 activity, and Hoechst staining assays. The intra-cellular reactive oxygen species level and expression level of the *CASP3* gene in AGS cells treated with ZnO@Gln-TSC NPs were evaluated.

Results: The NPs were in the size range of 20 to 70 nm. The DLS and zeta potential were 374 nm and -31.7 mV, respectively. In MTT, the IC_{50} of ZnO, TSC, oxaliplatin, and ZnO@Gln-TSC NPs for AGS cells were 130, 80.5, 67.7, and 9.8 µg/mL, respectively, and the IC_{50} of ZnO and ZnO@Gln-TSC NPs for HEK293 cells were 215 and 150.5 µg/mL, respectively. Flow cytometry showed higher apoptosis in the cell treated with the NPs and TSC. Apoptotic features, including cell shrinkage, were recognized. A significant increase of 5.9 folds in the level of ROS was noticed. The activity of caspase-3 and the expression level of the *CASP3* gene were increased by1.83 and 1.6 folds after exposure to ZnO@Gln-TSC NPs, respectively.

Conclusions: This study revealed the anti-cancer potential of ZnO@Gln-TSC NPs to be used for gastric cancer treatment after further *in vitro* and *in vivo* assays.

Keywords: Apoptosis, gastric cancer, nanoparticle, thiosemicarbazide, zinc oxide

Address for correspondence: Dr. Ali Salehzadeh, Department of Biology, Rasht Branch, Islamic Azad University, Rasht, Iran.
E-mail: salehzadeh@iaurasht.ac.ir
Submitted: 17-Oct-2023; **Revised:** 14-Feb-2024; **Accepted:** 17-Feb-2024; **Published:** 26-Aug-2024

Introduction

According to the global cancer burden, based on the GLOBOCAN 2021, 19.3 million new cancer cases and almost 10.0 million cancer deaths were estimated in 2020. Gastric cancer remains an important cancer worldwide and is responsible for over 1 million new cases in 2020 and an estimated 769,000 deaths (equal to one in 13 deaths, globally), ranking fifth for incidence and fourth for cancer mortality.[1] A large number of drugs in chemotherapy suffer from different shortcomings such as emerging multi-drug resistance (MDR), poor solubility, and undesirable damage to normal cells, which are commonly noticed in therapeutic interventions.[2] Recently,

Access this article online

Quick Response Code:

Website: www.advbiores.net

DOI: 10.4103/abr.abr_412_23

How to cite this article: Beigi S, Salehzadeh A, Habibollahi H, Sadat Shandiz SA, Safa F. The effect of ZnO nanoparticles functionalized with glutamine and conjugated with thiosemicarbazide on triggering of apoptosis in the adenocarcinoma gastric cell line. Adv Biomed Res 2024;13:72.

the development of metal nanoparticles (NPs) has gained consideration due to their potential in cancer diagnosis, tumor imaging, and drug delivery.[3] Thiosemicarbazones (TSCs) are a sub-class of iron-chelating agents that are believed to have anti-cancer activity. The high potential for the application of this compound class can be illustrated by the fact that the TSCs have been used in clinical trials. Latest studies confirmed the anti-cancer effect of TSC-metal compounds in comparison to TSC alone. TSC can form stable complexes with metals such as Ag, Fe, Zn, Ga, and Cu.[4] So, it is possible to use the ZnO-TSC complex in biomedical and diagnostic fields and as a drug delivery agent, for instance, polymeric micelles, liposomes, dendrimers, and colloidal gold, which are used in directed tumor treatments. The metal-TSC composite, on active directing, can attach to their receptors expressed on the cancer cells' surface.[5] There are studies that were led to evolve new metal-TSC complexes and their potential considering anti-cancer properties.[5,6]

The increase in the prevalence of gastric carcinoma and the ineffectiveness of existing methods and, on the other hand, the significant advances in nanotechnology in the diagnosis and treatment of cancer have led researchers to find new treatment methods using metal NPs and combine them with substances with anti-cancer properties. Since ZnO NPs and TSC each alone have shown anti-cancer properties, now, this study deals with the effect of combining these two substances together and evaluating their anti-cancer potential in gastric cancer cells.

So here, the ZnO@Gln-TSC NPs were synthesized through functionalization of ZnO NPs using glutamine (Gln), and then, ZnO@Gln was conjugated by TSC. The final product was characterized by various physico-chemical methods. The IC_{50} of ZnO@Gln-TSC for AGS and HEK293 cell lines was determined by MTT assay. Ultimately, the apoptogenic effect of ZnO@Gln-TSC was evaluated by flow cytometry, staining of cells by Hoechst33258 dye, intra-cellular reactive oxygen species (ROS) level, caspase-3 activity, and the expression level of the *CASP3* gene in NP-treated cells.

Materials and Methods

Reagents

$Zn(NO_3)_2 6H_2O$, thiosemicarbazide, glutamine, oxaliplatin, phosphate-buffered saline (PBS), MTT solution, and dimethyl sulfoxide (DMSO) were purchased from Sigma-Aldrich company (USA).

ZnO and ZnO@Gln-TSC NP synthesis

For the synthesis of ZnO NPs, 300 mg of $Zn(NO_3)_2 6H_2O$ was dissolved in 300 mL of dH_2O and the pH was adjusted to 11. The mixture was stirred at 80°C for 2 hours. Next, the mixture was centrifuged and the precipitate was washed with dH_2O. For the synthesis of ZnO@Gln, 300 mg of $Zn(NO_3)_2 6H_2O$ and 150 mg of glutamine were dissolved in 300 mL of dH_2O and the pH was adjusted to 11. The mixture was stirred at 80°C for 2 hours. Next, this mixture was centrifuged and the pellet was washed with dH_2O. To synthesize the final product (ZnO@Gln-TSC), 300 mg of ZnO@Gln and 500 mg of thiosemicarbazide were dissolved in 200 mL of dH_2O and stirred at 40°C for 24 hours, and then, the NPs were collected, washed with dH_2O, and dried at 80°C.[6]

Characterization of ZnO@Gln-TSC NPs

The ZnO@Gln and ZnO@Gln-TSC NPs were analyzed by Fourier transform infrared (FT-IR) spectroscopy using a Nicolet IR 100 spectrophotometer at a wavelength range from 400 to 4500 cm^{-1}.

X-ray diffraction analysis (XRD) was used to recognize the crystalline structure of ZnO@Gln-TSC NPs (Philips X'Pert MPD, Netherlands). The size and shape of ZnO@Gln-TSC NPs were evaluated using scanning electron microscopy (SEM) (TESCAN MIRA3, Czech Republic) and transmission electron microscopy (TEM) (ZEISS EM 900, Germany). Energy-dispersive X-ray (EDX) mapping analysis was employed to detect the elemental composition of ZnO@Gln-TSC (TESCAN MIRA3, Czech Republic). The hydrodynamic size, stability, dispersion, and electrostatic repulsion of ZnO@Gln-TSC NPs were evaluated using DLS and zeta potential analyses (Malvern Panalytical, UK).

Maintenance of cell lines

The *in vitro* anti-proliferative activity of ZnO@Gln-TSC NPs was assessed using human gastric carcinoma AGS (CRL-1739) cells and human embryonic kidney HEK293 (ATCC CRL-1573), non-tumor cells, which were purchased from the National Cell Bank of Iran.

The cell lines were maintained in Dulbecco's modified Eagle's medium (DMEM) supplemented with 10% (v/v) fetal bovine serum (FBS) and 1% penicillin/streptomycin (antibiotic solution). The T-25 culture flasks were used to keep the cells at 37°C in a 5% carbon dioxide (CO_2) and 95% humidity atmosphere.

To change the cell culture medium, the previous medium was first removed and the flask containing AGS cells was washed with PBS (37°C). Then, 2 mL of trypsin was added to the medium to cover the surface of the cells and placed in the incubator for 3–5 minutes to separate the membrane connections of AGS cells from the surface of the flask. To neutralize trypsin, 2 mL of the culture medium was added to the flask. The solution containing the cells was poured into a 15 mL Falcon tube and centrifuged for 5 minutes at 1000 RPM, and the supernatant was separated. The resulting pellet was suspended in 3 mL of the culture medium, and then, 2 ml of the cell suspension was seeded in the T25cell culture flask containing 5 ml of the culture medium. These steps were repeated once every 3 days until the cells were ready for the next tests.

In order to count the cells, trypsinization and separation of cells from the surface of the flask were done first. Then, 3 mL of the complete culture medium was added to the solution containing cells. The cells were centrifuged at 1000 RPM for

5 minutes, the supernatant was separated, and the cell pellet was suspended in 3 mL of the culture medium.

To prepare 500 µL of the cell-dye solution, 400 µL of Trypan Blue solution was added to 100 µL of the cell solution and mixed. Next, 100 µL of the mixture was poured on a hemocytometer slide. The number of cells in each slide zone was counted using an objective microscope with 100X magnification, and the average number of cells in four zones was calculated. A fivefold dilution of the cell suspension with Trypan Blue dye was performed, so the obtained number is multiplied by 5 to obtain the number of cells in a 1 mL scale. The average number of cells required for each well is 1×10^4 cells/mL.

MTT assay

The *in vitro* toxicity of ZnO, TSC, ZnO@Gln-TSC, and oxaliplatin for AGS and HEK293 cells was determined using the 3-[4, 5-dimethylthiazol-2-yl]-2, 5-diphenyltetrazolium bromide (MTT) colorimetric assay.[7] 96-well microplates were used to propagate the cells with a density of 1×10^4 and incubated overnight (37°C) with a series of dilutions (15.625, 31.25, 62.5, 125, 250, 500 µg/mL) of ZnO, TSC, ZnO@Gln-TSC, and oxaliplatin for AGS cells. Meanwhile, in the same concentration, the cytotoxicity of ZnO NPs and ZnO@Gln-TSC NPs toward HEK293 cells was evaluated.

Then, 20 µL of MTT solutions (5 mg/mL in PBS) was added to the growth medium of treated cells. The medium in each well was replaced with 100 µL of DMSO to dissolve formed formazan crystals. Subsequent to shaking for 15 min, the absorbance of the solution was evaluated at 570 nm using a microplate reader (UV-1601, Shimadzu, Kyoto, Japan). The experiment was done in six replicates.

Finally, the cell viability percentage was calculated according to the following formula:

$$(\%)\ \text{Cell viability} = \frac{\text{Absorbance of Treated cells}}{\text{Absorbance of Control cells}} \times 100$$

Hoechst 33258 staining

The apoptosis patterns in ZnO@Gln-TSC NP-treated AGS cells were evaluated using the Hoechst 33258 staining. The AGS cells were grown in 6-well plates with a density of 5×10^3 for 24 h and exposed to 9.8 µg/mL of ZnO@Gln-TSC. Subsequent to washing with PBS, the cells were fixed by 4% formaldehyde and then incubated with Hoechst 33258 for 15 min and in darkness. Finally, the cells were examined using a fluorescence microscope (Zeiss, Wetzlar, Germany).

Annexin V-FITC/PI apoptosis detection

AGS cells were grown in 6-well plates with a density of 5×10^3 and treated with 80.5 µg/mL of TSC and 9.8 µg/mL of ZnO@Gln-TSC NPs for 24 hours, and the Annexin V-FITC (5 µL) and propidium iodide (10 µL) stains were then added to the AGS cells, which were treated with TSC and ZnO@Gln-TSC and incubated for 10 min in darkness. The viable, early apoptotic, late apoptotic, and necrotic cells were screened by flow cytometry.

Intra-cellular ROS level

The generation of ROS in NP-treated and control cells was quantified by a flow cytometry assay using an ROS detection kit (Abcam Inc, USA). AGS cells were grown in 6-well plates with a density of 5×10^3 and treated with 9.8 µg/mL of ZnO@Gln-TSC NPs for 24 h. Then, 2′, 7′-dichlorofluorescein diacetate (DCF-DA) (20 mM) was added to the wells and incubated at 37°C for 24 h in darkness. Finally, the ROS level was quantified using a flow cytometry device.

Caspase-3 activity

The activity of caspase-3 in NP-treated and control cells was quantified using a commercial kit (ApoTarget™Caspase assay, Invitrogen Corp, USA). AGS cells were seeded in 6-well plates with a density of 5×10^3, treated with 9.8 µg/mL of ZnO@Gln-TSC NPs for 24 h, and then subjected to caspase-3 activity assay according to the manufacturer's instruction. After incubation for 2 h, the optical absorbance was measured at 400 nm. The untreated AGS cells were considered controls.

Expression of CASP3 gene by real-time PCR

Real-time PCR was used to evaluate the level of caspase-3 gene expression. At first, AGS cells were cultured in 6-well plates with a density of 5×10^3. Based on the results of the MTT test, the cells were treated with ZnO@Gln-TSC NPs with a concentration of 9.8 µg/mL and incubated for 24 hours at 37°C. Extraction of total RNA was carried out using the Qiagen kit, RNeasy Plus Mini Kit (Valencia, CA), and using the manufacturer's instructions. After RNA extraction, synthesis of complementary DNA was performed using a PrimeScriptTM first strand cDNA Synthesis Kit (Takara, Tokyo, Japan). Finally, the expression level of the *CASP3* gene was compared to that of the *GAPDH* gene as an internal control gene. The assay was performed in triplicates using specific primers for each gene using the SYBR Green® Premix Ex TaqTM kit (TaKaRa, Japan) and ABI 7300 real-time PCR thermal cycler (Applied Biosystems, Foster City, CA). The final volume of the reaction mixture was 20 µL and contained 10 µL of SYBR Green master mix, 1 µL of each primer, 2 µL of template cDNA, and 6 µL of distilled water. The gene amplification program includes the initial denaturation stage (95°C/10 minutes) and then 40 cycles of denaturation (95°C/15 seconds), annealing (60°C/60 seconds), and elongation (72°C/45 seconds). Evaluation of gene expression compared to the control gene was done based on the $2^{-\Delta\Delta Ct}$ method. The sequence of primers for the *CASP3* gene is F: GCCTGCCGTGGTACAGAACT, R: GCACAAAGCGACTGGATGAAC. Also, the sequence of primers for the *GAPDH* gene is F: CCCACTCCTCCACCTTTGAC, R: CATACCAGGAAATGAGCTTGACAA.[8]

Statistical analysis

One-way ANOVA and T-test analyses were performed using SPSS (version 16.0) software to check the statistical differences, and a *P* value of less than 0.05 was considered as the significance level.

Results

FT-IR spectra analysis

Figure 1a and 1b illustrate the FT-IR spectra for ZnO@Gln and ZnO@Gln–TSC nanostructures, respectively. The spectrum in Figure 1a displays a characteristic band at 430–530 cm^{-1} belonging to the stretching vibrations of the Zn-O bond, confirming the successful synthesis of ZnO NPs.[9] The band observed at ~3430 cm^{-1} is assigned to the hydroxyl groups of the adsorbed water molecules onto the zinc oxide NPs.[10] Similar bands exist in the spectrum of ZnO@Gln–TSC given in Figure 1b. The metal oxide stretching band can be observed at 491 cm^{-1} with a considerable decrease in the intensity because of the functionalization of ZnO NPs by glutamine. Additionally, a more intense and broader band is observed for the -OH group due to overlapping with the stretching vibrations of the hydroxyl and amine groups in the amino acid. Figure 1b also indicates some additional peaks belonging to the glutamine moiety of the ZnO@Gln–TSC nanomaterial. The sharp absorption peak observed at 3630 cm^{-1} can be attributed to the free -NH stretching vibration mode of glutamine, and the peak located at 1384 cm^{-1} is assigned to the C-N stretching vibrations of the amide group.[11] Moreover, the indicator signal of the charged NH_3^+ group of the amino acid is observed at about 2100 cm^{-1}.[12] The intense peak located at 1626 cm^{-1} belongs to the asymmetric stretching vibrations of $–COO^–$ groups of glutamines, indicating its anionic nature.[13] The peaks at 1025 and 1040 are also assigned to the C-N stretching vibrations of the amine group in glutamine.[14] Finally, the band located at 1117 cm^{-1} is attributed to the stretching vibrations of the C-O group. Notably, the band at ~1170 cm^{-1} indicates the presence of the C=S group of thiosemicarbazide,[15] which confirms the involvement of TSC on the surface of the nanomaterial.

XRD analysis

The crystalline nature of the synthesized nanostructures was investigated by recording the XRD pattern in the angle range (2θ) of 20°–80°. Figure 2 illustrates the XRD patterns of ZnO@Gln-TSC. The results show the characteristic peaks of ZnO NPs at 31.57°, 34.27°, 36.07°, 47.47°, 56.47°, 62.78°, 66.52°, 67.87°, 68.97°, 72.42°, and 77.17°, which can be assigned to the crystallographic orientation of 100, 002, 101, 102, 110, 103, 112, 200, 201, 004, and 202, respectively.[16,17] The narrow and intense peaks show high purity and the crystalline structure of the NPs, which are consistent with the wurtzite phase of zinc oxide (JCPDS Card No. 36-1451). The findings clearly confirmed that ZnO@Gln-TSC NPs were successfully synthesized.

Electronic microscope and EDX analysis

The morphology and particle size of the ZnO@Gln-TSC NPs were checked out using SEM and TEM. SEM and TEM micrographs showed that the synthesized ZnO@Gln-TSC NPs

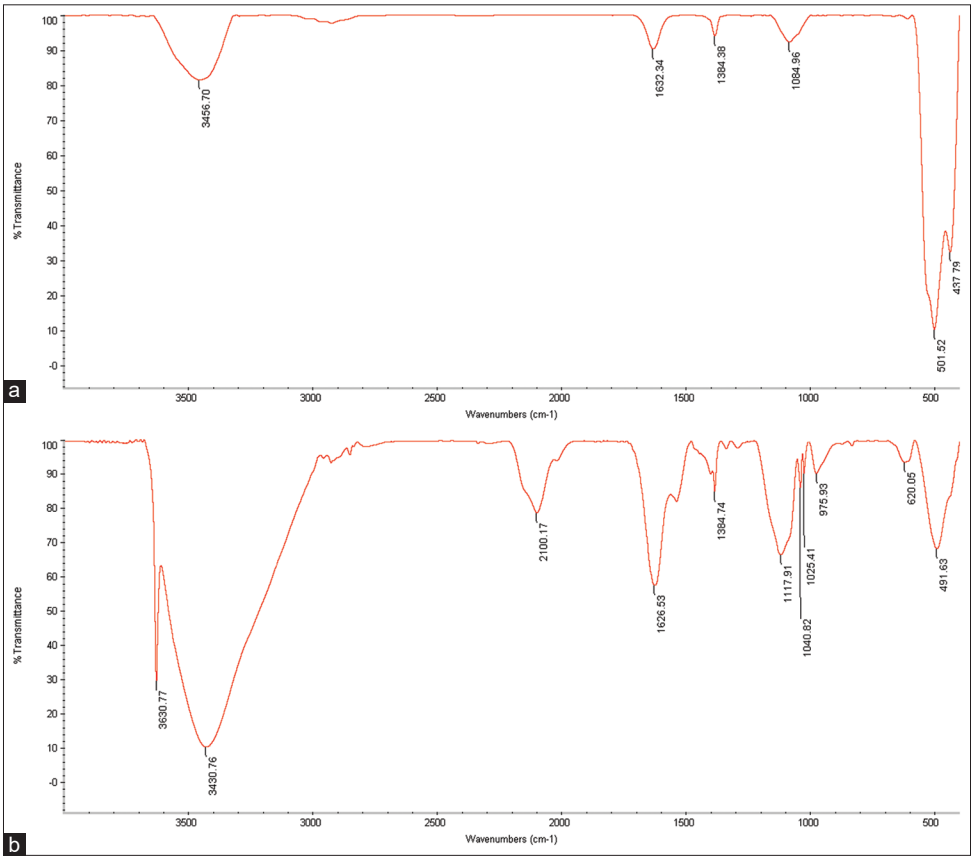

Figure 1: FT-IR spectra for ZnO@Gln (a) and ZnO@Gln–TSC (b) nanostructures. The absorption peaks of these two graphs indicate the stretching vibrations of COO - C-N - C-O - and the presence of C-S and NH_2 groups

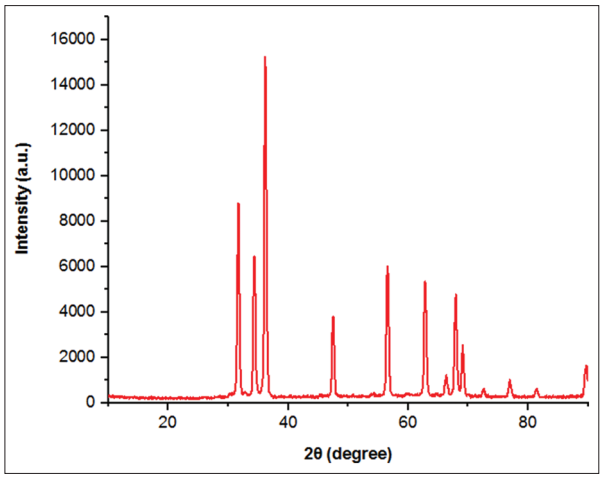

Figure 2: XRD patterns of ZnO@Gln-TSC. The diffraction peaks correspond to the reflection pattern confirming the crystallographic surfaces of ZnO@Gln-TSC NPs

had a particle size between 20 and 70 nm for SEM and between 50 and 70 nm for TEM [Figure 3a and b].

The synthesized ZnO@Gln-TSC NPs were characterized by EDX analysis to clarify their elemental composition. As can be observed in Figure 4a and 4b, the presence of Zn, S, O, C, and N atoms was confirmed without elemental impurity.

DLS analysis and zeta potential analysis

DLS analysis was conducted to evaluate the size and distribution of particle diameter in the produced NPs. Based on the result of the DLS histogram, the mean diameter of ZnO@Gln-TSC NPs was 374 nm [Figure 5a]. The zeta potential measurement for ZnO@Gln-TSC NPs was −31.7 mV, which provides electrostatic repulsion between the NPs [Figure 5b].

Analysis of the cytotoxicity of NPs by MTT assay

To explore the cytotoxicity of NPs on cell lines, the MTT assay was used in the cells treated with gradient concentrations of ZnO NPs, TSC, ZnO@Gln-TSC NPs, and oxaliplatin. According to the MTT results, ZnO@Gln-TSC NPs significantly declined the viability of AGS cells in a dose-dependent lethal activity.

The IC_{50} concentrations of ZnO NPs, TSC, ZnO@Gln-TSC NPs, and oxaliplatin against AGS cells were 130, 80.5, 9.8, and 67.7, respectively. Also, the IC_{50} of ZnO and ZnO@Gln-TSC NPs on the normal (HEK293) cell line were 215 µg/mL and 150.5 µg/mL, respectively [Figure 6] (*: *P* value < 0.01, **: *P* value < 0.05, ***: *P* value < 0.001).

Hoechst 33258 and Annexin V-FITC/PI staining analysis

To evaluate the apoptogenic property of ZnO@Gln-TSC NPs, Hoechst 33258 staining was used. Following overnight treatment of AGS with 9.8 µg/mL of ZnO@Gln-TSC NPs, apoptotic properties including cell shrinkage, fragmented nuclei, and nuclear consolidation were recognized. Control cells indicate an intact and normal morphology [Figure 7a and b], while we have noticed morphological changes in ZnO@Gln-TSC NP-treated AGS cells, causing stimulation of apoptosis pathways.

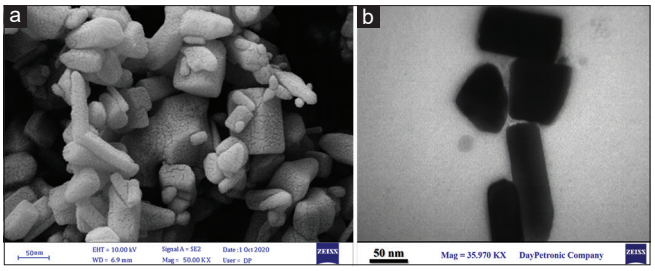

Figure 3: Morphological and particle size of the ZnO@Gln-TSC NPs can be observed in (a) SEM and (b) TEM images. The size of ZnO@Gln-TSC NPs in the SEM imaging is in the range of 20 to 70 nm, and in the TEM imaging, it is in the range of 50 to 70 nm

The Annexin V-FITC/PI staining method was carried out to evaluate apoptosis induction levels by ZnO@Gln-TSC NPs. The untreated control AGS cells consisted of 91.5% viable cells, 1.03% early apoptosis, 1.17% late apoptosis, and 6.26% cell necrosis [Figure 8a]. Treatment with 9.8 µg/mL of ZnO@Gln-TSC NPs led to changes in the proportions to 33.3% for viable cells, 55.5% for early apoptosis, 9.48% for late apoptosis, and 1.77% for necrotic cells [Figure 8b]. For TSC group, untreated control AGS cells consisted of 97.51% viable cells, 0.81% early apoptosis, 0.06% late apoptosis, and 1.62% necrotic cells [Figure 8c]. Treatment with 80.5 µg/mL of TSC led to changes in the proportions to 78.46% for viable cells, 15.21% for early apoptosis, 2.43% for late apoptosis, and 3.90% for necrotic cells [Figure 8d].

ROS level analysis

To evaluate the effect of ZnO@Gln-TSC NPs on the generation of oxidative stress, the levels of intra-cellular ROS molecules in NP-treated and control cells were quantified. The mean fluorescent intensity in the control group was 82.1, while in ZnO@Gln-TSC NPs, treated cells increased to 484, which indicates the effect of the NPs on the generation of oxidative stress [Figure 9].

Analysis of the activity of caspase-3 protein and change of CASP3 gene expression

Measuring the activity of caspase-3 protein showed that treating with ZnO@Gln-TSC NPs caused a considerable increase (1.83 folds) in the activity of caspase-3 in AGS cells (**: *P* value < 0.05) [Figure 10].

The level of *CASP3* gene expression was investigated after treatment of AGS cells with ZnO@Gln-TSC NPs at a concentration of 9.8 µg/mL using the real-time PCR technique. The results showed that the exposure of AGS cells to the NPs caused an increase in the *CASP3* gene expression compared to the control group by 1.6 folds. The results are shown in Figure 11 (**: *P* value < 0.05).

Discussion

Due to the complexity of cancer drug resistance, it is necessary to examine new and promising treatment strategies with fewer side effects.[18] ZnO nanostructures are widely used materials

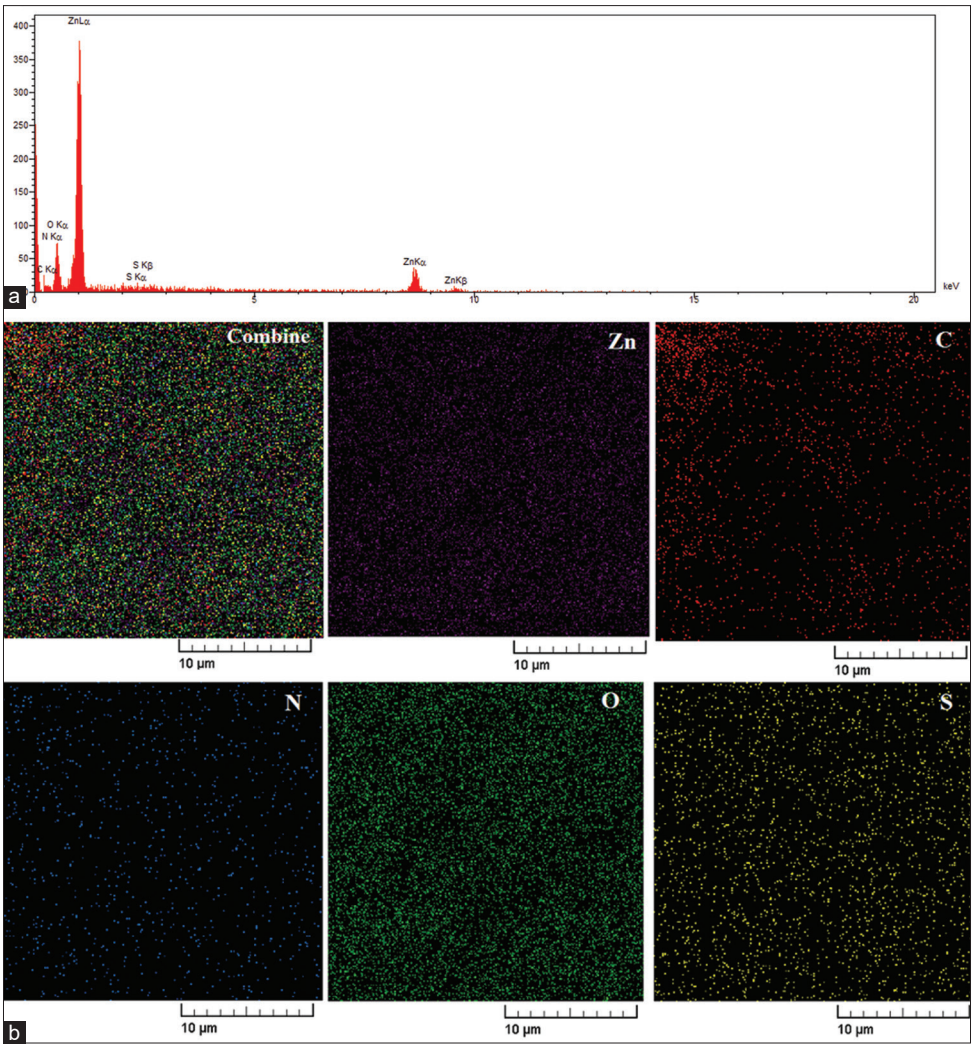

Figure 4: The diagram (a) and constituent elements of ZnO@Gln-TSC NPs (b) were characterized by EDX. The results of this test confirm the presence of N, C, Zn, S, and O elements in the synthesized NPs

in a variety of fields, including agriculture, cosmetics, food, and medicine.[19] Herein, we produced novel ZnO@Gln-TSC NPs, which could efficiently exert anti-cancer properties on gastric cancer cells. In our study, glutamine was used for two purposes; the first goal was to use it as a bridge molecule to improve the conjugation of ZnO NPs and thiosemicarbazide. The second aim was to provide targeted delivery of ZnO NPs and thiosemicarbazide to cancer cells. Several studies have shown that glutamine is a major nutrient involved in multiple aspects of cancer metabolism. Glutamine is the most abundant amino acid in the blood and muscle and is largely exploited for energy generation and as a precursor for the biomass required for rapid cancer cell proliferation. In addition to providing a carbon source, glutamine metabolism also acts as a source of nitrogen for the synthesis of nucleic acids and other amino acids and also participates in the regulation of cellular redox homeostasis through a variety of mechanisms. Therefore, most cancer cells are dependent on glutamine and cannot live in the vacancy of exogenous glutamine, which is called "glutamine addiction".[20] In the meantime, penetration of ZnO@Gln-TSC NPs into cancer cells leads to cell death due to the anti-cancer activity of thiosemicarbazide. A large number of reports are available on exploring the anti-cancer properties of metallic NPs against various mammalian cell lines such as MNK45 human gastric cancer[21] and breast cancer cell lines.[22] Apoptosis induction by zinc oxide NPs has been investigated in MCF7, MDA-MB-231 breast cancer cells,[23] H82, and H187 human small-cell lung cancer cells.[24] *Morus nigra*-loaded zinc oxide NPs were able to reduce the cell viability against AGS gastric cancer cells with an IC_{50} level of 10 µg/mL after 24 h treatment.[25] However, the anti-cancer effects of the ZnO@Gln-TSC NPs on human cell lines have not been explored yet. Nejabatdoust *et al*. showed that ZnO@Glu-TSC NPs have synergistic anti-microbial properties against MDR *S. aureus* strains.[6,26] In our study, we found that treatment with ZnO@Glu-TSC NPs reduced viability of gastric cancer cells, which suggests that ZnO@Gln-TSC NPs can reduce the growth of cancerous cells.

Apoptotic cells display different morphological characteristics including membrane blebbing, cell shrinkage, appearance of

apoptotic bodies, and chromosome condensation by triggering specific signaling pathways.[27] Previous investigation showed that the conjugated thiosemicarbazide with NPs has an improved anti-cancer effect on human cancer cells, which support this study. It has been reported that cobalt oxide NPs functionalized by glutamic acid (Glu) and conjugated with thiosemicarbazide (TSC) complex had promising cytotoxic effects on the gastric cancer (AGS) cell line.[28] Similarly, Abbaszadeh *et al*. showed that the conjugated thiosemicarbazide with nickel oxide NPs induced cell apoptosis in MCF-7 (human breast cancer) cells.[29] However, no investigation has been performed on the apoptotic properties of ZnO@Gln-TSC NPs against gastric cancer cell lines. We observed that the ratio of cell apoptosis was increased in ZnO@Gln-TSC NPs and TSC-treated groups compared to the control group. A previous investigation reported that Co_3O_4@Glu-TSC NPs have cytotoxic effects on AGS human gastric cancer cells. In that work, the IC_{50} value of Co_3O_4@ Glu-TSC NPs toward human AGS cells was 107.5 µg/mL and the late apoptosis level was 8.85%. In contrast, the late apoptosis level was higher in our study (28%), while the IC_{50} value was lower than that reported byJarestan *et al*. results. These results suggest that ZnO@Gln-TSC NPs are more efficient than Co_3O_4@Glu-TSC NPs against AGS cells.[28] The generation of oxidative stress is considered a major contributing mechanism to the anti-cancer effect of metal NPs. We found that treatment of AGS cells with ZnO@Gln-TSC NPs caused a significantly increased generation of ROS molecules. Several studies reported that the generation of ROS molecules is a common outcome of exposure to metal NPs.[30,31] Akhtar *et al*. demonstrated that ZnO NPs selectively induce apoptosis in cancer cells, which is likely to be mediated by ROS that can trigger pro-apoptotic pathways, which is in agreement with our finding. Upon the induction of oxidative stress and thus reduced activity of the glutathione peroxidase (GSH), damage to cell components occurs, which results in the activation of pro-apoptotic factors, including caspases and p53 protein.[32] Therefore, the induction of oxidative stress by the generation of ROS molecules could

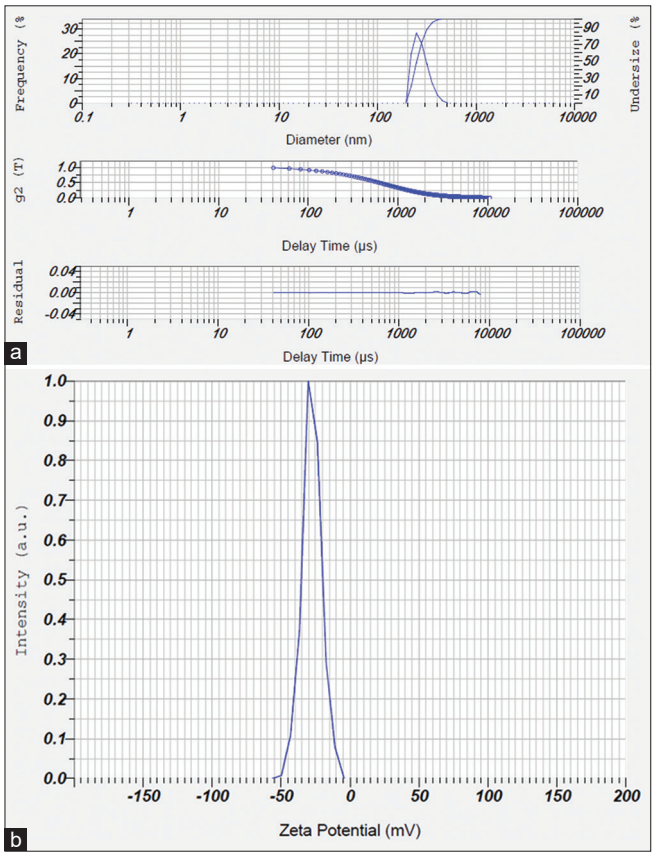

Figure 5: DLS (a) and zeta potential (b) measurement of ZnO@Gln-TSC NPs. The average particle size of ZnO@Gln-TSC NPs in the DLS test is 374. The zeta potential test graph of the ZnO@Gln-TSC NP showed -31.7 mV

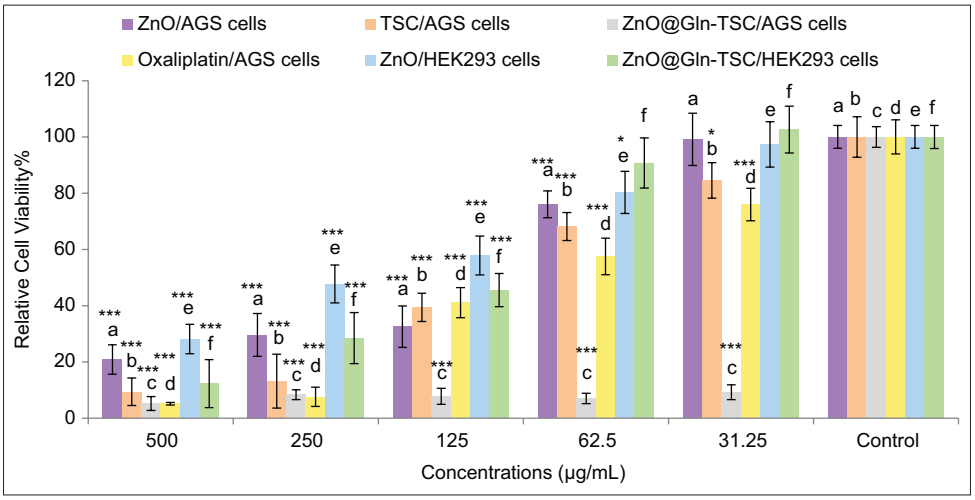

Figure 6: *In vitro* toxicity effect of ZnO NPs (a), TSC (b), ZnO@Gln-TSC NPs (c), and oxaliplatin (d) against the AGS cell line. Also, the toxicity effect of ZnO NPs (e) and ZnO@Gln-TSC NPs (f) on HEK293 cell line (*: *P*-value < 0.01, **: *P*-value < 0.05, ***: *P*-value < 0.001). The MTT assay showed that the cell proliferation of AGS cells decreased in a dose-dependent manner. At a concentration of 500 µg/mL, the greatest inhibition was observed. The IC_{50} Of ZnO NPs, TSC, oxaliplatin, and ZnO@Gln-TSC NP on AGS cells were 130 µg/mL, 80.5 µg/mL, 9.8 µg/mL, and 67.7 µg/mL, respectively. The IC_{50} concentration of ZnO NPs and ZnO@Gln-TSC NPs were 215 µg/mL and 150.5 µg/mL in normal HEK293 cells

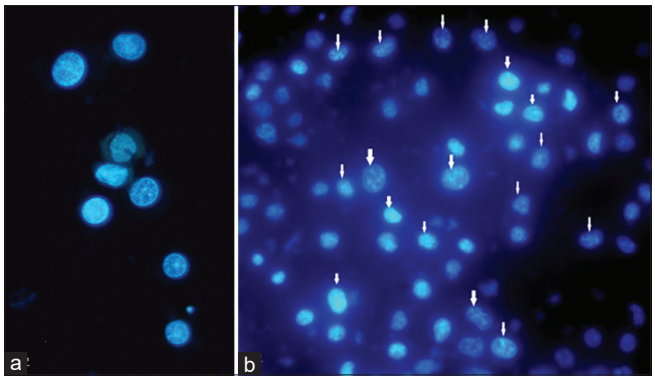

Figure 7: Morphological changes of AGS cells with Hoescht 33258 staining: (a) Untreated as control and (b) treated with an IC50 concentration of synthesized ZnO@Gln-TSC NPs (9.8 μg/mL) for 24 hours. The arrows show the apoptotic cells. Apoptotic properties including cell shrinkage, fragmented nuclei, and nuclear consolidation were recognized.

be considered a therapeutic strategy to treat cancers. Due to abnormal metabolism in cancer cells, they have generally a higher ROS content compared to normal cells. Therefore, the increased level of ROS due to exposure to ZnO@Gln-TSC NPs could result in higher susceptibility to the exogenous ROS induction.[33] Caspase-3 is the main mediator caspase that is activated through both intrinsic and extrinsic apoptotic pathways. Measuring the activity of caspase-3 is an important indicator of the progression of cell apoptosis. Due to the key role of caspase-3 in protein cleavage in cell apoptosis, the increased activity of this protease in NP-treated cells confirms the progression of apoptotic pathways, which is in agreement with the results from the flow cytometry assay.[34] The current study revealed that ZnO@Gln-TSC NPs could up-regulate caspase-3 activity in AGS cells. Our data comply with previous reports, which suggested that ZnONPs could be potent inducers of caspase-9 and caspase-3 expression at protein and mRNA levels

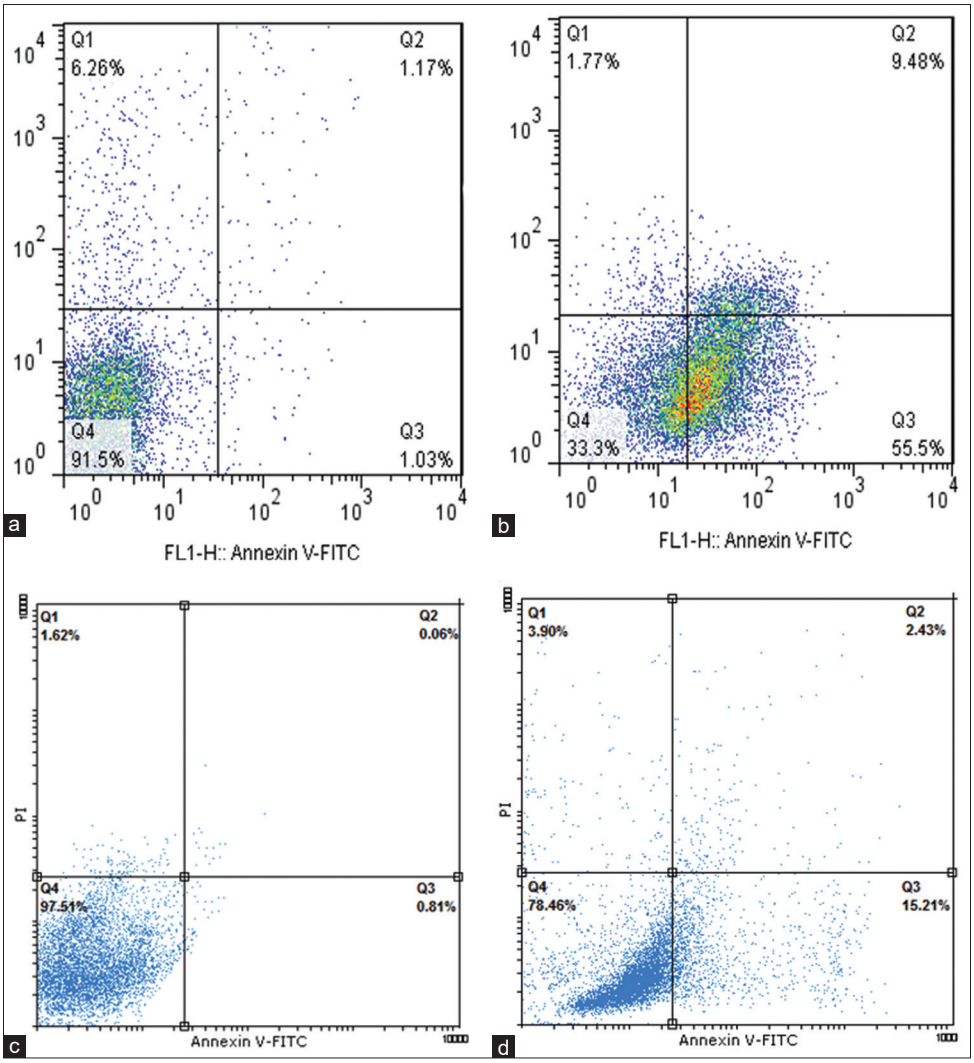

Figure 8: Flow cytometric analysis by annexin V/PI staining test for ZnO@Gln-TSC NPs group: untreated control (a) and treated AGS cells (b) after 24 hours of incubation. This test was performed at an IC_{50} concentration of 9.8 μg/mL of ZnO@Gln-TSC NPs in AGS cancer cells and in the control group. About 55.5% of the cells have undergone early apoptosis, and 9.48% have undergone delayed apoptosis. Also, the flow cytometric analysis for TSC (IC_{50} of 150 μg/mL) presented untreated cells (c) and treated cells (d) after 24 hours of incubation. About 15.21% of the cells have undergone early apoptosis, and 2.43% have undergone delayed apoptosis

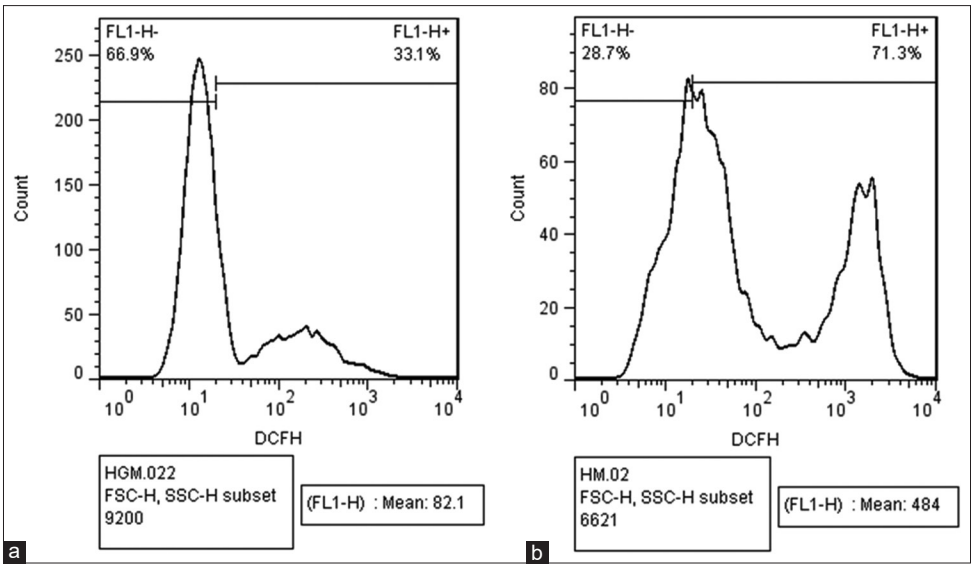

Figure 9: Intracellular ROS levels control (a) and ZnO@Gln-TSC NPs (b) treated AGS cells. The results indicate that treating with the NPs leads to a significant increase in the generation of ROS molecules

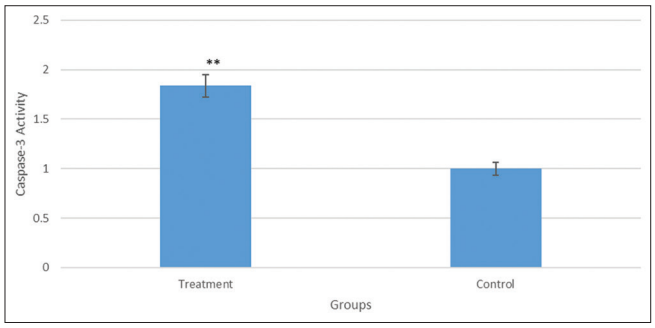

Figure 10: Comparison of the activity of caspase-3 in AGS cells treated with ZnO@Gln-TSC NPs and control cells. Upon treatment with ZnO@Gln-TSC NPs, activity of the enzyme significantly increased by 1.83 folds (**: *P*-value < 0.05)

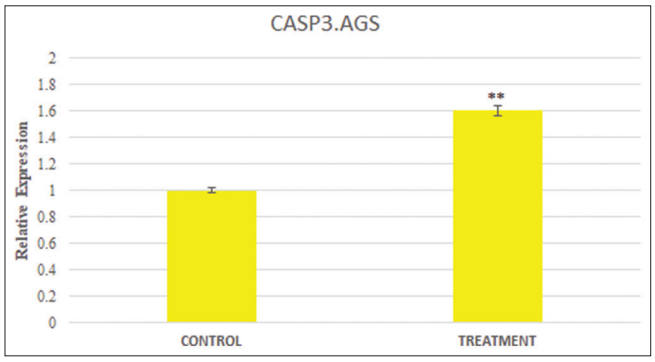

Figure 11: Investigating *CASP3* gene expression in cells exposed to ZnO@Gln-TSC NPs compared to control group cells. Exposure of AGS cells to ZnO@Gln-TSC NPs led to a significant increase of 1.6 folds in *CASP3* gene expression compared to control cells (**: *P*-value < 0.05)

in human multiple myeloma cells.[35,32] The results of real-time PCR assay showed that the expression of the *CASP3* gene, as one of the most important genes involved in the apoptotic cascade, was increased in NP-treated cells. The results of the caspase-3 activity test and the expression level of the *CASP3* gene indicate the activation of the programmed death pathway in the cells treated with ZnO@Gln-TSC NPs.[36] Thiosemicarbazones can increase the expression of the suppressor gene NDRG1, which plays a role in inhibiting tumor growth, tumor progression, and angiogenesis. The complex of ZnO NPs and thiosemicarbazone induces the production of ROS and leads to the activation of the P53 pathway, the regulation of BCL2 family proteins, inhibition of the cell cycle in the S phase, and apoptosis.[37,38]

Zinc oxide NPs can decrease the mRNA expression of inflammatory cytokines by inhibiting the activation of NF-kB. Recent studies have shown that the conjugation of thiosemicarbazide or its derivatives to metal NPs can improve their stability as well as increase their anti-tumor and anti-cancer properties.[39]

By inhibiting enzymes related to nucleic acid replication, such as topoisomerases, thiosemicarbazide can disrupt the process of cell DNA replication. It has also been reported that thiosemicarbazide causes DNA damage, membrane damage, and dysfunction of enzyme structures.[40,41]

On the other hand, metal NPs damage cell structures such as the cytoplasmic membrane and nucleic acids by stimulating the production of oxygen free radicals and causing oxidative stress, thus causing the death of cancer cells.[42]

Based on the results of this study, ZnO@Gln-TSC NPs effectively prevented the proliferation of AGS cancer cells, and with increasing concentration of the NPs, the survival rate of cells decreased.

Based on our results, zinc oxide NPs and thiosemicarbazide individually have less anti-cancer effects on AGS cells than ZnO@Gln-TSC NPs. Studies have shown that despite the anti-cancer effect potential of thiosemicarbazones,

they cannot inhibit cancer cells individually. Conjugating thiosemicarbazide or its derivatives to metal NPs can lead to improved stability as well as increased anti-tumor and anti-cancer properties.[39] It has been found that the conjugation of thiosemicarbazide to zinc oxide NPs, which are linked together through amino acids, can improve penetration of the NPs into cancer cells and enhance anti-cancer potential against AGS cells.[43]

Conclusion

In summary, ZnO@Gln-TSC NPs were synthesized by the co-precipitation method and physicochemical analyses confirmed the identity of the obtained NPs. The results of *in vitro* cytotoxicity assay, flow cytometry, Hoescht 33258 staining, intra-cellular ROS level, the activity of caspase-3 protein, and also the expression level of the *CASP3* gene indicated that the fabricated ZnO@Gln-TSC NPs could act as a promising compound in treating gastric cancer in future.

Financial support and sponsorship

Nil.

Conflicts of interest

There are no conflicts of interest.

References

1. Sung H, Ferlay J, Siegel RL, Laversanne M, Soerjomataram I, Jemal A, *et al*. Global cancer statistics 2020: GLOBOCAN Estimates of incidence and mortality worldwide for 36 cancers in 185 countries. CA Cancer J Clin 2021;71:209-49.
2. Medarova Z, Pantazopoulos P, Yoo B. Screening of potential miRNA therapeutics for the prevention of multi-drug resistance in cancer cells. Sci Rep 2020;10:1970.
3. Lu L, Kang S, Sun C, Sun C, Guo Z, Li J, *et al*. Multifunctional nanoparticles in precise cancer treatment: considerations in design and functionalization of nanocarriers. Curr Top Med Chem 2020;20:2427-41.
4. Akladios FN, Andrew SD, Parkinson CJ. Cytotoxic activity of expanded coordination bis-thiosemicarbazones and copper complexes thereof. J Biol Inorg Chem 2016;21:931-44.
5. Kalinowski DS, Quach P, Richardson DR. Thiosemicarbazones: The new wave in cancer treatment. Future Med Chem 2009;1:1143-51.
6. Nejabatdoust A, Salehzadeh A, Zamani H, Moradi-Shoeili Z. Synthesis, characterization and functionalization of ZnO nanoparticles by glutamic acid (Glu) and conjugation of ZnO@ Glu by thiosemicarbazide and its synergistic activity with ciprofloxacin against multi-drug resistant *Staphylococcus aureus*. J. Clust. Sci 2019;30:329-36.
7. Kang T, Guan R, Chen X, Song Y, Jiang H, Zhao J. *In vitro* toxicity of different-sized ZnO nanoparticles in Caco-2 cells. Nanoscale Res Lett 2013;8:496.
8. Bigdeli R, Shahnazari M, Panahnejad E, Cohan RA, Dashbolaghi A, Asgary V. Cytotoxic and apoptotic properties of silver chloride nanoparticles synthesized using *Escherichia coli* cell-free supernatant on human breast cancer MCF 7 cell line. Artif Cells Nanomed Biotechnol 2019;47:1603-9.
9. Ramesh P, Saravanan K, Manogar P, Johnson J, Vinoth E, Mayakannan M. Green synthesis and characterization of biocompatible zinc oxide nanoparticles and evaluation of its antibacterial potential. Sens. Bio-Sens. Res 2021;31:100399.
10. Khurana N, Arora P, Pente AS, Pancholi KC, Kumar V, Kaushik CP, Rattan S. Surface modification of zinc oxide nanoparticles by vinyltriethoxy silane (VTES). Inorg. Chem. Commun 2021;124:108347.
11. Senthilkumar SR, Sivakumar T. Green tea (Camellia sinensis) mediated synthesis of zinc oxide (ZnO) nanoparticles and studies on their antimicrobial activities. Int J Pharm Pharm Sci. 2014;6:461-5.
12. Pawlukojć A, Hołderna-Natkaniec K, Bator G, Natkaniec I. L-glutamine: Dynamical properties investigation by means of INS, IR, RAMAN, 1H NMR and DFT techniques. Chem. Phys 2014;443:17-25.
13. Barrak H, Saied T, Chevallier P, Laroche G, M'nif A, Hamzaoui AH. Synthesis, characterization, and functionalization of ZnO nanoparticles by N-(trimethoxysilylpropyl) ethylenediamine triacetic acid (TMSEDTA): Investigation of the interactions between Phloroglucinol and ZnO@ TMSEDTA. Arab. J. Chem 2019;12:4340-7.
14. Jamdagni P, Khatri P, Rana JS. Green synthesis of zinc oxide nanoparticles using flower extract of Nyctanthes arbor-tristis and their antifungal activity. J. King Saud Univ. Sci 2018;30:168-75.
15. Dehkaei AA, Khalatbari K, Emamifar A, Taramsari SM, Balkhi S, Ghezeljeh SM, *et al*. Cytotoxicity effect of nickel hydroxide nanoparticles functionalized by glutamine and conjugated by thiosemicarbazide on human lung cancer cell line (A549) and evaluation of bax and bcl-2 genes expression. Gene Rep 2022;29:101700.
16. Gupta K, Chundawat TS. Zinc oxide nanoparticles synthesized using Fusarium oxysporum to enhance bioethanol production from rice-straw. Biomass and Bioenergy. 2020;143:105840.
17. Sarkar S, Sarkar R. Synthesis, characterization and tribological study of zinc oxide nanoparticles. Materials Today: Proceedings. 2021;44:3606-12.
18. Mansoori B, Mohammadi A, Davudian S, Shirjang S, Baradaran B. The Different Mechanisms of Cancer Drug Resistance: A Brief Review. Adv Pharm Bull 2017;7:339-48.
19. Subhan MA, Neogi N, Choudhury KP. Industrial Manufacturing Applications of Zinc Oxide Nanomaterials: A Comprehensive Study. Nanomanufacturing 2022;2:265-91.
20. Altman BJ, Stine ZE, Dang CV. From Krebs to clinic: Glutamine metabolism to cancer therapy. Nat Rev Cancer 2016;16:619-34.
21. Hashemi SF, Tasharrofi N, Saber MM. Green synthesis of silver nanoparticles using Teucrium polium leaf extract and assessment of their antitumor effects against MNK45 human gastric cancer cell line. Mol. Struct 2020;1208:127889.
22. Karuppaiya P, Satheeshkumar E, Tsay HS. Biogenic synthesis of silver nanoparticles using rhizome extract of Dysosma pleiantha and its antiproliferative effect against breast and human gastric cancer cells. Mol Biol Rep 2019;46:4725-34.
23. Boskabadi SH, Balanezhad SZ, Neamati A, Tabrizi MH. The green-synthesized zinc oxide nanoparticle as a novel natural apoptosis inducer in human breast (MCF7 and MDA-MB231) and colon (HT-29) cancer cells. Inorg. Nano-Met. Chem 2020;51:733-43.
24. Tanino R, Amano Y, Tong X, Sun R, Tsubata Y, Harada M, *et al*. Anticancer activity of zno nanoparticles against human small-cell lung cancer in an orthotopic mouse model. Mol Cancer Ther 2020;19:502-12.
25. Tang Q, Xia H, Liang W, Huo X, Wei X. Synthesis and characterization of zinc oxide nanoparticles from Morus nigra and its anticancer activity of AGS gastric cancer cells. J Photochem Photobiol B 2020;202:111698.
26. Nejabatdoust A, Zamani H, Salehzadeh A. Functionalization of ZnO nanoparticles by glutamic acid and conjugation with thiosemicarbazide alters expression of efflux pump genes in multiple drug-resistant *staphylococcus aureus* strains. Microb Drug Resist 2019;25:966-74.
27. Chen Q, Kang J, Fu C. The independence of and associations among apoptosis, autophagy, and necrosis. Signal Transduct Target Ther 2018;3:18.
28. Jarestan M, Khalatbari K, Pouraei A, Sadat Shandiz SA, Beigi S, Hedayati M, *et al*. Preparation, characterization, and anticancer efficacy of novel cobalt oxide nanoparticles conjugated with thiosemicarbazide. 3 Biotech 2020;10:230.
29. Abbaszadeh N, Jaahbin N, Pouraei A, Mehraban F, Hedayati M, Majlesi A, *et al*. Preparation of Novel Nickel Oxide@ Glutamic/ Thiosemicarbazide Nanoparticles: Implications for Cytotoxic and Anti-cancer Studies in MCF-7 Breast Cancer Cells. J. Clust. Sci 2021;22:1-9.
30. Lin LS, Wang JF, Song J, Liu Y, Zhu G, Dai Y, *et al*. Cooperation of endogenous and exogenous reactive oxygen species induced by zinc peroxide nanoparticles to enhance oxidative stress-based cancer therapy. Theranostics 2019;9:7200-9.

31. Khalid AD, Ur-Rehman N, Tariq GH, Ullah S, Buzdar SA, Iqbal SS, *et al*. Functional bioinspired nanocomposites for anticancer activity with generation of reactive oxygen species. Chemosphere 2023;310:136885.
32. Akhtar MJ, Ahamed M, Kumar S, Khan MM, Ahmad J, Alrokayan SA. Zinc oxide nanoparticles selectively induce apoptosis in human cancer cells through reactive oxygen species. Int J Nanomedicine 2012;7:845-57.
33. Zou Z, Chang H, Li H, Wang S. Induction of reactive oxygen species: An emerging approach for cancer therapy. Apoptosis 2017;22:1321-35.
34. Badrooh M, Shokrollahi F, Javan S, Ghasemipour T, Rezaei Mojdehi S, Farahnak H, *et al*. Trigger of apoptosis in adenocarcinoma gastric cell line (AGS) by a complex of thiosemicarbazone and copper nanoparticles. Mol Biol Rep 2022;49:2217-26.
35. Li Z, Guo D, Yin X, Ding S, Shen M, Zhang R, *et al*. Zinc oxide nanoparticles induce human multiple myeloma cell death via reactive oxygen species and Cyt-C/Apaf-1/Caspase-9/Caspase-3 signaling pathway *in vitro*. Biomed Pharmacother 2020;122:109712.
36. Kaushik NK, Kaushik N, Wahab R, Bhartiya P, Linh NN, Khan F, *et al*. Cold atmospheric plasma and gold quantum dots exert dual cytotoxicity mediated by the cell receptor-activated apoptotic pathway in glioblastoma cells. Cancers (Basel) 2020;12:457.
37. Gou Y, Wang J, Chen S, Zhang Z, Zhang Y, Zhang W, *et al*. A-N-heterocyclic thiosemicarbazone Fe (III) complex: Characterization of its antitumor activity and identification of anticancer mechanism. Eur J Med Chem 2016;123:354-64.
38. Goya GF, Grazu V, Ibarra MR. Magnetic nanoparticles for cancer therapy. Curr. Nanosci 2008;4:1-16.
39. Hamrayev H, Shameli K, Yusefi M. Preparation of zinc oxide nanoparticles and its cancer treatment effects: A review paper. Journal of Advanced Research in Micro and Nano Engineering 2020;2:1-11.
40. Habibzadeh SZ, Salehzadeh A, Moradi-Shoeili Z, Shandiz SAS. A novel bioactive nanoparticle synthesized by conjugation of 3-chloropropyl trimethoxy silane functionalized Fe (3) O (4) and 1-((3-(4-chlorophenyl)-1-phenyl-1H-pyrazol-4-yl)methylene)-2-(4-phenylthiazol-2-yl) hydrazine: Assessment on anti-cancer against gastric AGS cancer cells. Mol Biol Rep 2020;47:1637-47.
41. Richardson DR, Sharpe PC, Lovejoy DB, Senaratne D, Kalinowski DS, Islam M, *et al*. Dipyridyl thiosemicarbazone chelators with potent and selective antitumor activity form iron complexes with redox activity. J Med Chem 2006;49:6510-21.
42. Bejarbaneh M, Moradi-Shoeili Z, Jalali A, Salehzadeh A. Synthesis of Cobalt Hydroxide Nano-flakes Functionalized with Glutamic Acid and Conjugated with Thiosemicarbazide for Anticancer Activities Against Human Breast Cancer Cells. Biol Trace Elem Res 2020;198:98-108.
43. El-Boubbou K. Magnetic iron oxide nanoparticles as drug carriers: Preparation, conjugation and delivery. Nanomedicine (Lond) 2018;13:929-52.